Materials Science & Engineering A 735 (2018) 260–268

Contents lists available at ScienceDirect

Materials Science & Engineering A

journal homepage: www.elsevier.com/locate/msea

Experimental and numerical simulation analysis on creep crack growth behavior of CLAM steel

Y. Zhao, S. Liu*, J. Shi, X. Mao

Key Laboratory of Neutronics and Radiation Safety, Institute of Nuclear Energy Safety Technology, Chinese Academy of Sciences, Hefei, Anhui 230031, China

ARTICLE INFO

Keywords:
Creep crack growth
*C** parameter
Microstructure evolution
CLAM steel

ABSTRACT

The experiment and numerical simulation were performed to analyze the creep crack growth behavior of China Low Activation Martensitic (CLAM) steel under temperatures ranging from 500 °C to 600 °C with a step of 50 °C. The creep crack growth micro-mechanism under multiaxial state of stress was investigated with the compact tension (CT) specimens. The creep crack growth rates were simulated based on the Nikbin-Smith-Webster (NSW) model. The difference of the crack propagation behavior is correlated with the evolution of two types of precipitates: Cr-rich $M_{23}C_6$ and W-rich M_6C phases. The coarsening of $M_{23}C_6$ carbides and the precipitation of M_6C phase particles lead to dissolving of the solid solution elements and deteriorating the creep properties during the testing processes.

1. Introduction

Fusion energy can provide a CO_2 emission-free, sustainable energy, and has been considered as a radical option for the future energy requirement [1–4]. Reduced Activation Ferritic-Martensitic (RAFM) steels are considered as one kind of structural materials for the future fusion reactor for their high resistance to irradiation swelling, low-activation features, good thermal properties and mature industrial base [5–7]. China Low Activation Martensitic (CLAM) steel [8–12], one kind of the RAFM steels, was developed at the Institute of Nuclear Energy Safety Technology, Chinese Academy of Sciences. It has been chosen as the candidate structural material for the China test blanket module of ITER (ITER CN TBM), and the breeder blanket of the China fusion engineering test reactor.

The operating temperature faced by the RAFM steel in the fusion system is about 500 °C for a long time; therefore, the viscoplastic performance of materials has become a crucial consideration in order to prevent creep failure [13,14]. In the past years, the creep rupture behavior under uniaxial stress state of the RAFM steel has been studied by many researchers [15–19]. However, the different loading conditions and geometric discontinuity generate multi-axial stress state in the components [20]. It is therefore necessary to investigate the creep deformation behavior under the multiaxial stress state in order to understand the creep failure mechanisms and to predict the life of high temperature components in the future fusion reactors [20]. The creep crack growth tested with the compact tension specimens is an effective way to study the crack formation and crack growth behavior under the multi-axial stress state [21,22]. The creep crack initiation time and the crack propagation rate are important contents for the structural integrity assessment of the components in the nuclear reactor [23].

In the current research, the CLAM steel was studied with the compact tension (CT) specimens to determine the creep crack growth behavior under different testing conditions. The creep crack growth rate was stimulated based on the Nikbin-Smith-Webster (NSW) model with the results of a single uni-axial creep test. The propagation process of the creep crack was explained based on the change of microstructure near the crack tip.

2. Experimental

The research material is the CLAM steel (HEAT 0912). The main chemical compositions are listed in Table 1. The specimens were normalized at 980 °C for 30 min and tempered at 760 °C for 90 min, both followed by air cooling. The creep crack growth specimen was fabricated based on ASTM E 1457 [24] with a thickness of 10 mm, as shown in Fig. 1. A side-grooved with 20% of the thickness was introduced to constrain the crack growth route in the specimen. The detail parameters of creep crack growth experiments are shown in Table 2.

The fracture morphology at different test conditions was analyzed with Zeiss Sigma SEM Scanning Electron Microscope (SEM) operated at 15 kV to expound the mechanisms of the creep crack growth process. The microstructures of the CLAM steel before and after the test were

* Corresponding author.
E-mail address: shaojun.liu@fds.org.cn (S. Liu).

https://doi.org/10.1016/j.msea.2018.08.048
Received 17 April 2018; Received in revised form 13 August 2018; Accepted 14 August 2018
Available online 17 August 2018
0921-5093/

Table 1
The main chemical compositions of the steel (wt%).

Element	Cr	W	Mn	V	Ta	C	N	Fe
Content	8.86	1.48	0.48	0.21	0.12	0.094	0.011	Bal.

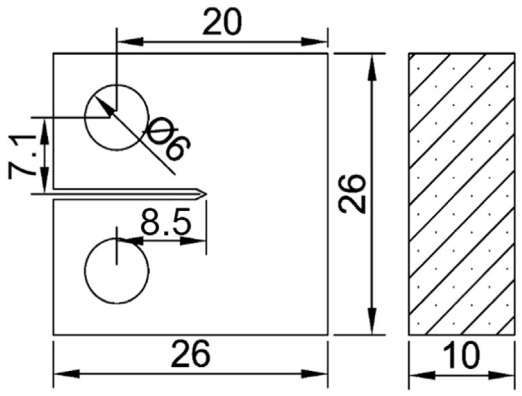

Fig. 1. The geometry and dimensions of the compact tension specimen (unit: mm).

Table 2
The parameters of creep crack growth experiment.

Sample No.	Temperature (°C)	Load (N)	Pre-crack length (mm)	Initial stress intensity factor (MPa $m^{1/2}$)
CT1	500	5, 000	2.50	49.16
CT2	550	4, 000	2.43	32.68
CT3[a]	550	4, 000	2.50	33.05
CT4	550	5, 000	2.58	41.91
CT5	550	6, 050	2.51	50.05
CT6	600	3, 650	2.48	30.10

[a] CT3 was suspended at 666.95 h to analyze the behavior of crack propagation.

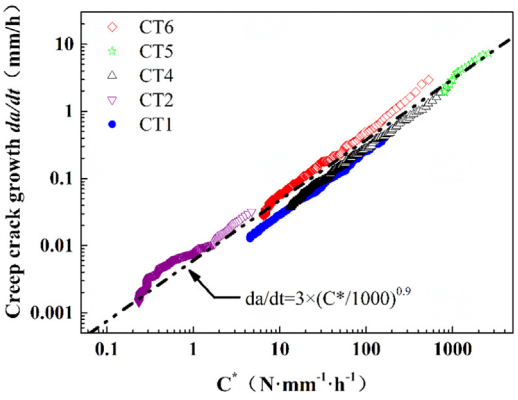

Fig. 3. The creep crack growth rate vs. C* at different testing conditions.

observed with an FEI Tecnai G2 F20 S-TWIN Transmission Electron Microscope (TEM) operated at 200 kV, the precipitates were identified based on the metallic elements composition measured by the Energy Dispersive Spectrometer (EDS). The dislocation density was analyzed with the line intersection method [25], and the precipitates were counted based on the method described in Ref. [26].

3. Results and discussion

3.1. Creep crack growth behavior

The creep crack length and the creep crack growth rate versus time under different testing conditions are given in the review literature [8] to introduce the research progress of CLAM steel. There are three different stages during the creep crack growth process: the crack incubation period, the steady growth period and the accelerated growth period. The incubation period increases with reducing the applied stress and the testing temperature and the initial crack growth rate increases with the increasing of the testing temperature and initial loading. The incubation period has been considered as the progress to build up creep damage to a steady state distribution at the crack tip. Increasing the

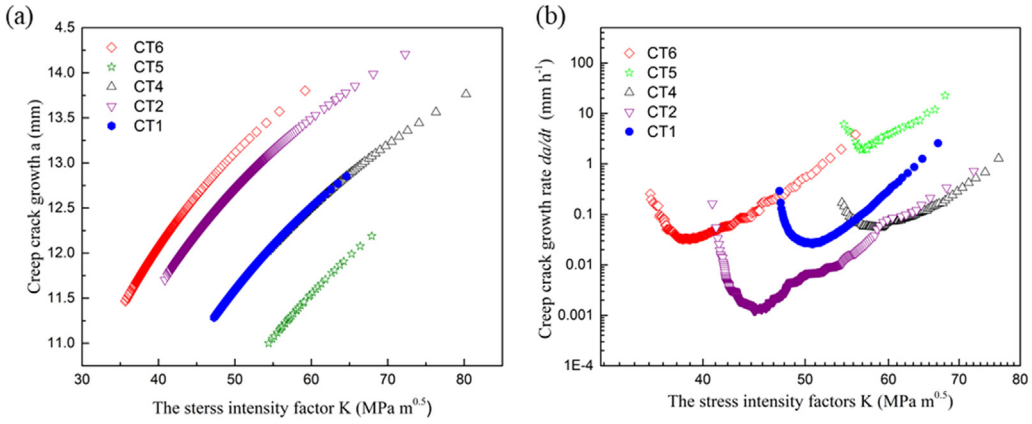

Fig. 2. Creep crack length (a) and creep crack growth rates (b) vs. the stress intensity factor at different temperatures and loads.

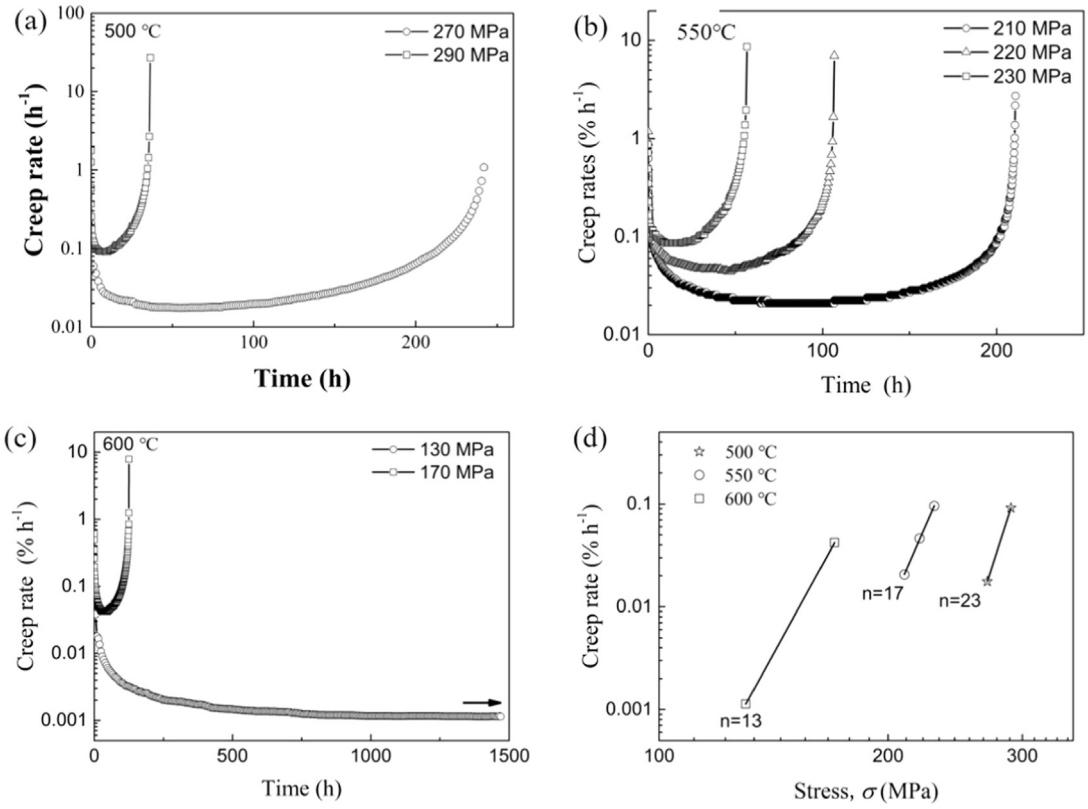

Fig. 4. The creep rate vs. time: (a), (b), (c) and (d) the creep rate vs. the stress.

Table 3
The condition of uniaxial creep test and Norton exponent, creep rupture strain.

Temperature T (°C)	Stress σ (MPa)	Min. creep rate $\dot{\varepsilon}_{min}$ (%/h)	Creep fracture strain ε_f	Norton exponent, n
500	270	0.01764	26.3%	23
	290	0.09177	26.7%	
550	210	0.02058	29.1%	17
	220	0.04606	29.5%	
	230	0.09587	29.6%	
600	130	0.04200	33.6%	13
	170	0.001135	33.9%	

Table 4
The Norton exponent and creep rupture strain.

Temperature (°C)	Norton exponent *n*	ε_f^*	Stress condition	NSW model
500	23	0.265	Plane stress	$\dot{a} = 11.3 \times \left(\frac{C^*}{1000}\right)^{0.958}$
		0.00530	Plane strain	$\dot{a} = 566 \times \left(\frac{C^*}{1000}\right)^{0.958}$
550	17	0.294	Plane stress	$\dot{a} = 10.2 \times \left(\frac{C^*}{1000}\right)^{0.944}$
		0.00588	Plane strain	$\dot{a} = 510 \times \left(\frac{C^*}{1000}\right)^{0.944}$
600	13	0.338	Plane stress	$\dot{a} = 8.88 \times \left(\frac{C^*}{1000}\right)^{0.929}$
		0.00676	Plane strain	$\dot{a} = 444 \times \left(\frac{C^*}{1000}\right)^{0.929}$

applied stress and temperature would accelerate the deform process near the crack tip, then shorten the time for the crack incubation period.

The creep crack length and creep crack growth rates under different applied temperatures and loads are shown in Fig. 2. The creep crack growth behavior in Fig. 2 is a typical feature for heat-resistant martensitic steels containing dispersed particles [27]. The minimum creep crack growth rate increases from ~ 0.001 mm*h^{-1} to 4 mm*h^{-1} with an increase in the applied load from 4, 000 N to 6, 050 N. The creep crack length is in a good agreement under the same stress intensity factor with 500 °C and 550 °C, as shown in Fig. 2(a). The consistent behavior of the creep cracks growth rate is obviously dependent on the testing temperature. Increasing the testing temperature would boost the creep zone near the crack tip. The linear elastic stress intensity factor, K, is suitable for describing the creep-brittle cracking behavior. For creep-ductile materials under steady state creep conditions, however, the linear elasticity may no longer be applicable and the stress intensity factor do not properly characterize crack growth rates. The crack tip stress and strain rate fields of ductile materials under steady crack growth are characterized by the parameter C* which can consider the influences of the load level and temperature [28].

The C^* parameter is used to describe the creep crack growth rates, which is calculated based on the displacement rates of the load line during the creep crack growth process [29]. For the CT specimens, the C^* is shown as Eq. (1):

$$C^* = \frac{P\dot{V}_c}{B_n(W-a)}\frac{n}{n+1}\left(2 + 0.522\frac{W-a}{W}\right) \quad (1)$$

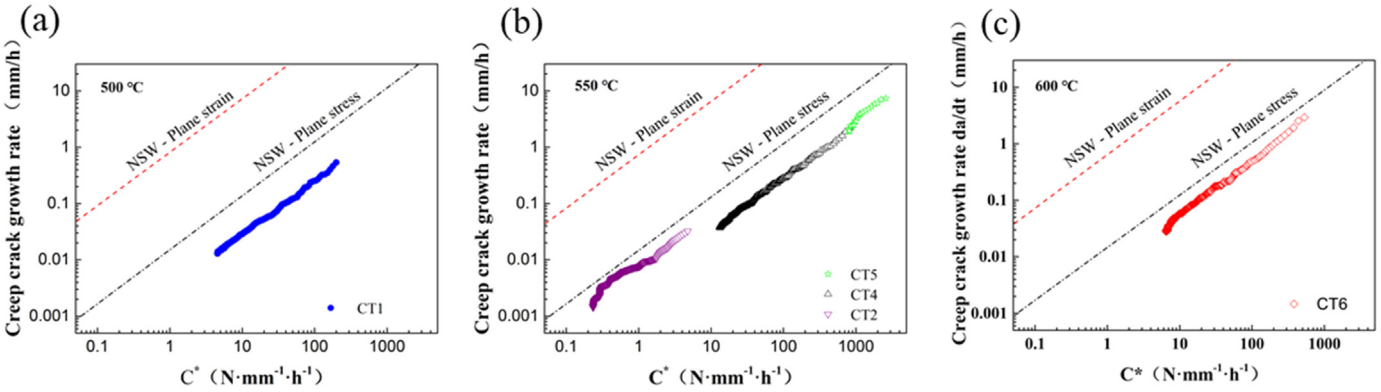

Fig. 5. Comparison of measured and predicted results of NSW model at different temperatures: (a) at 500 °C; (b) at 550 °C; (c) at 600 °C.

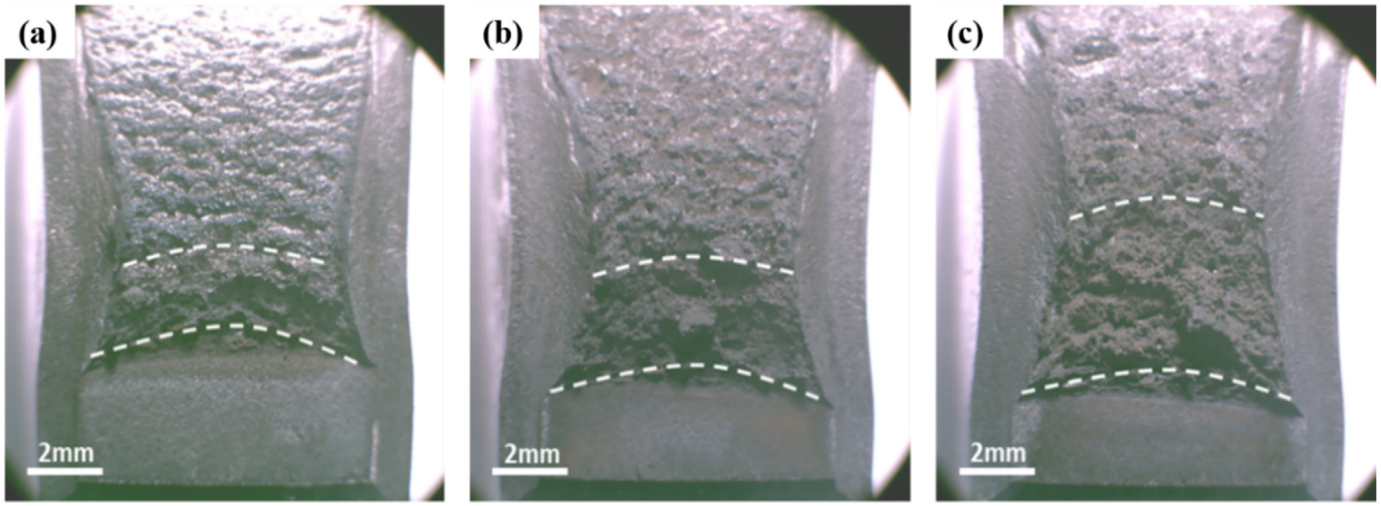

Fig. 6. The fracture morphology after the creep crack growth experiment: (a) 500 °C, (b) 550 °C, (c) 600 °.

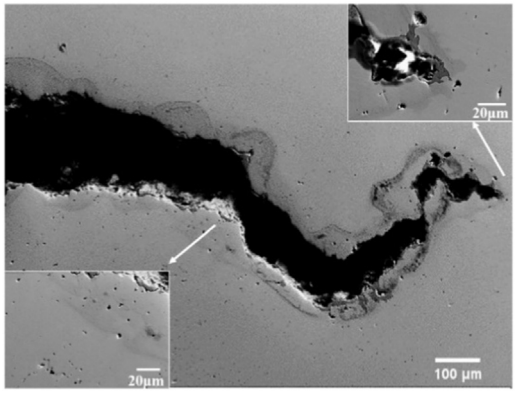

Fig. 7. The creep crack growth path at 550 °C, 4000 N.

where, $\dot{V_c}$ is the displacement rate of the load line, mm/h; n is the Norton exponent; P is the applied loading, N; a is the length of the crack, mm; B_n is the net thickness of the specimen, mm; and W is the wide of the specimen from the loading line, mm.

Fig. 3 shows the relationship between the creep crack growth rate and the C^* parameter, it presents a good proportional relationship under the logarithmic coordinates. The creep crack growth rates and C^* parameter increase during the experiment process. The applied stress and temperature have slight effects on the linear relationship, which means that the relationship can be described by the same equation. The relationship is given in Eq. (2) below:

$$da/dt = 3 \times \left(\frac{C^*}{1000}\right)^{0.9} \tag{2}$$

3.2. Model for creep crack growth of CLAM steel

The creep crack growth behavior of the CLAM steel was simulated based on NSW [30] model. Combined with the ductile depletion model, the crack tip Hutchinson-Rice-Rosengren (HRR) stress field and Cocks-Ashby model [31] were performed to assess the damage of the crack tip. The NSW model is shown in Eq. (3) as follows:

$$\dot{a} = \frac{3}{\varepsilon_f^*}\left(\frac{C^*}{1000}\right)^{\phi} \tag{3}$$

where, $\phi = n/(n+1)$, and n is the Norton exponent, the units of C* is N mm^{-1} h^{-1}, ε_f^* is the multi-axis creep fracture strain which can be calculated based on the uniaxial creep fracture strain [32]. The relationship is shown in the following Eq. (4):

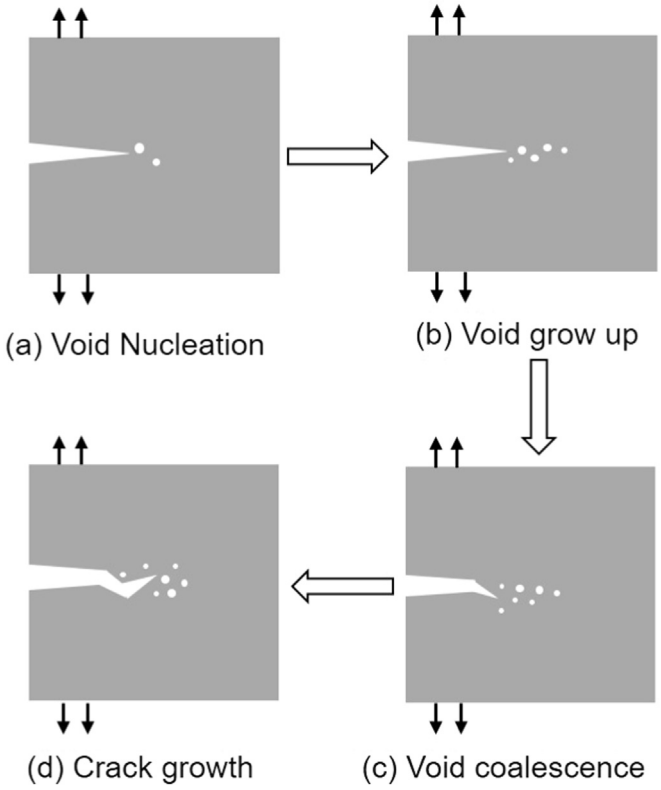

Fig. 8. The schematic diagram of creep crack growth.

$$\begin{cases} \varepsilon_f^* = \varepsilon_f, & \textit{for the plane stress} \\ \varepsilon_f^* = \frac{1}{50}\varepsilon_f, & \textit{for the plane stain} \end{cases} \quad (4)$$

To obtain the Norton exponent, n and creep fracture strain, ε_f of the CLAM steel, the uniaxial creep experiments were performed at 500 °C, 550 °C and 600 °C, respectively. Fig. 4 shows the creep rates versus time under different test conditions. The Norton exponent was calculated based on the Norton equation [33]. The creep rupture strain ε_f of the material was calculated by comparing the ratio of the elongation to the original length of the specimen. The experimental conditions and results are shown in Table 3, and the Norton exponent and creep rupture strain are listed in Table 4.

Fig. 5 shows the test results and predicted values based on the NSW model at different temperatures. It can be seen that the creep crack propagation rate is lower than that of the NSW model at all test conditions. The creep crack propagation rate predicted based on the plane strain condition is much larger than the experimental result, while the creep crack propagation rate in the plane stress state is close to the experimental result. As shown in Fig. 5(b), under the temperature for the plain stress condition, when the C* parameter is higher than 20, the predicted result is about four times of the test result; when the C parameter is less than 10, there is an only slight difference between the predicted result and the experimental result. From the above analysis, it can be seen that the NSW model based on the uniaxial tensile creep properties could be used to predict the creep crack propagation rate of the CLAM steel for the plain stress condition.

3.3. Microstructure mechanisms for creep crack growth

Fig. 6 shows the creep crack growth profiles. The creep crack growth zone was marked with the white dot line, and the creep crack growth zone increased with the temperature elevation. The higher testing temperature would facilitate the dislocations slide and increase the ductile of the CLAM steel, then enlarge the creep crack growth zone. All of the specimens have essentially "uniform" crack growth across the test section due to the side-grooved.

The CT3 specimen was suspended at 666.95 h to analyze the crack growth path during the creep experiment. The specimen was cut along the half thickness; and the microstructure is shown in Fig. 7. It can be seen that the creep crack propagated with twists and turns. There are a lot of creep pore on both sides of the crack and at the crack tip. Based on the microstructure, the creep crack growth pattern of the CLAM steel is shown in Fig. 8. At the later stage of the creep crack propagation period, the specimen gradually generated holes in the testing process. Creep voids continued to grow and connect with the main crack, then the crack extended forward, and eventually led to the fracture of the specimen.

3.4. Microstructure changes on creep crack growth

Many researches have shown that it is an ever-changing microstructure in the creep process caused by multi-factor processes, such as lath coarsen, decreased in dislocation density and variation of precipitates [34].

The lath structure of the steel after creep failure of CT1, CT4 and CT5 are shown in Fig. 9(a), (b), (c) and (d), respectively. The lath width was counted on 50 lathes. Extensive coarsen transformation of lath structure of sizes in between 0.4 and 0.5 μm were observed during creep exposure. The creep period may be the one of important factors for the coarsened processes, and increasing the temperature would improve the size distribution of the lath. The movement of Y-junction and recombination of two lath boundaries caused by the recovery of dislocations are considered as the main mechanism for the lath coarsening processes [35].

The change of dislocation density after the creep crack growth process is shown in Fig. 10. The dislocation density was decreased during the testing process, the testing temperature and time are the main effects of the change of dislocation. With the temperature increasing from 500 °C to 550 °C at 5, 000 N, the dislocation density decreases about an order. However, the increasing of stress shows less influence on the dislocation density; this different behavior of dislocation density may be caused by the decrease of the creep period at high stress level.

The precipitates evolution after creep crack growth process is shown in Fig. 11. There are two kinds of precipitates in the matrix, namely $M_{23}C_6$ and MX [36]. The larger precipitates (about 100–150 nm) were Cr-rich $M_{23}C_6$ carbides, and the smaller precipitates (about 40–50 nm) were Ta-rich MX particle. $M_{23}C_6$ carbides were precipitated along the prior austenite grain boundaries and lath boundaries, and MX particle were precipitated within laths. So, the $M_{23}C_6$ and MX precipitates were differentiated. After long time aging or creep testing, M_6C (Fe_3W_3C) carbide precipitates and Laves (Fe_2W) phase precipitates may be

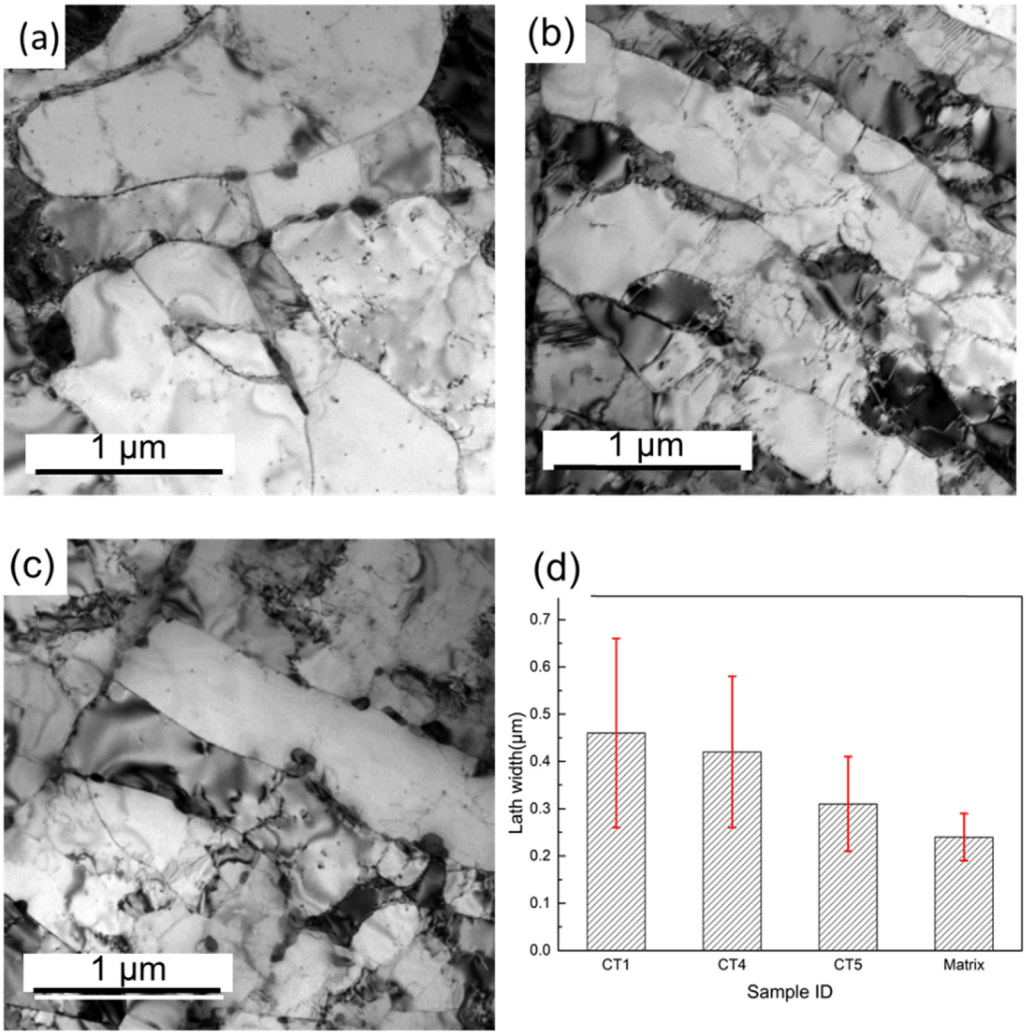

Fig. 9. The lath structure after creep crack growth process: (a) CT1; (b) CT4; (c) CT5; (d) the lath width of Matrix, CT1, CT4 and CT5.

observed in the matrix [37]. According to the atom ratio and composition observed with TEM/EDS, it could be supposed that the W-rich precipitate is M_6C carbide precipitates. The M_6C precipitates have also been detected under the similar condition in Eurofer 97 steels [38].

It has been found that $M_{23}C_6$ and MX carbides and M_6C phase particles have played an essential part in keeping the structure stability in the lath martensite [37]. Fig. 11 shows the size change of $M_{23}C_6$ carbides, MX carbonitrides, and M_6C phase particles of CT1, CT4 and CT5, respectively. Coarsening of $M_{23}C_6$ type of carbides was observed during the testing. The diameter of $M_{23}C_6$ precipitates was evaluated with the average size of 120 particles under the same testing conditions. It is observed that $M_{23}C_6$ carbides have coarsened to about 200–220 nm for the CT1, and to about 270–280 nm for CT4. MX type precipitates size has no significant change after the testing; similar behavior had been reported in previous studies [38].

The precipitation of W-rich M_6C [39] type particles were found after the testing process, as shown in Fig. 11. W is an important solid solution strengthening element for the CLAM steel, the formation of W-rich M_6C will deplete the W in the matrix and following with a loss of solid solution hardening effect; therefore, the W-rich M_6C formation and growth would be a reason for the properties degradation for the material servicing in the high temperature environment [40].

4. Conclusions

The creep crack growth behavior of the CLAM steel under the service temperatures ranging from 500 °C to 600 °C was investigated with the CT specimens. The temperature and magnitude of stress show significantly effect on the creep crack growth behavior, the conclusions are summarized as follows:

(1) The creep crack incubation period and steady-state propagation rate depend on testing temperatures and initial loads. The incubation period increases with reducing of the applied stress and the

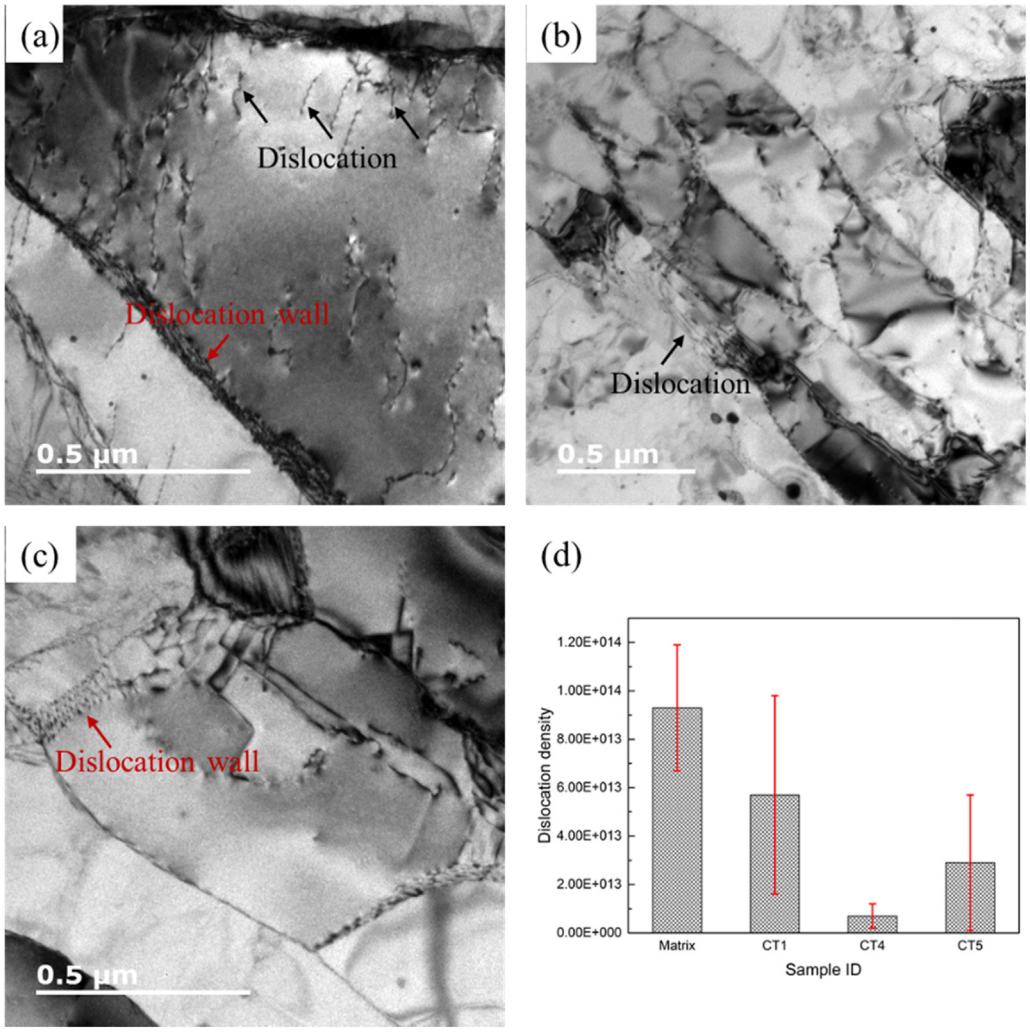

Fig. 10. The dislocation structure after creep crack growth process: (a) CT1; (b) CT4; (c) CT5; (d) the dislocation density of Matrix, CT1, CT4 and CT5.

testing temperature, and the steady-state propagation rate shows a positive correlation with the applied stress and the testing temperature.

(2) With the uniaxial tensile creep test data, the NSW model of creep crack propagation of the CLAM steel was established. The NSW model predicted results based on the plane stress condition are consistent with the experimental results for the CLAM steel.

(3) Increasing temperature would enhance the length of the creep crack zone in the CLAM steel. The holes nucleation, aggregation, and growth near the crack tip may be the mechanisms for the creep crack growth. The coarsening of $M_{23}C_6$ carbides and the precipitation of M_6C phase particles seem to be the principal reason for the creep properties degradation of the CLAM steel.

Acknowledgements

We would like to appreciate thank Prof. Q. Huang for the valuable comments and suggestions on the work, and thank K. Wang for the performed experiments, and also thank for the great help from the members of the FDS team in this research. Furthermore, this work is supported by the National Natural Science Foundation of China with Grant Nos. 51601190 and 11632001, the Youth Innovation Promotion Association of the Chinese Academy of Sciences with grant No. 2017486, the National Magnetic Confinement Fusion Science Program of China with Grant No. 2015GB109006, and the Chinese Academy of Sciences Pioneer Hundred Talents Program.

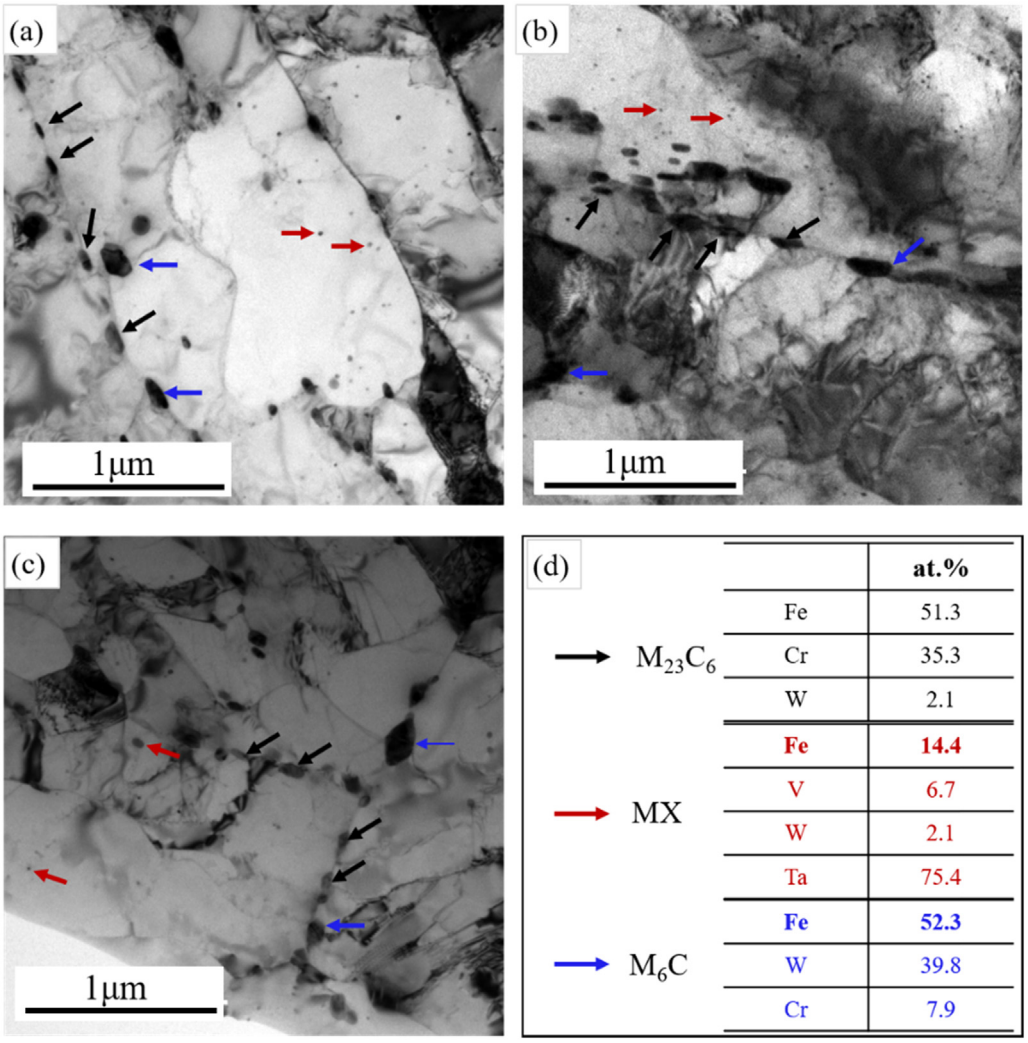

		at.%
$M_{23}C_6$	Fe	51.3
	Cr	35.3
	W	2.1
MX	**Fe**	**14.4**
	V	6.7
	W	2.1
	Ta	75.4
M_6C	**Fe**	**52.3**
	W	39.8
	Cr	7.9

Fig. 11. The precipitates evolution after creep crack growth process: (a) CT1; (b) CT4; (c) CT5; (d) the composition of precipitates analyzed with EDS.

References

[1] S.C. Cowley, The quest for fusion power, Nat. Phys. 12 (2016) 384–386.
[2] Y. Wu, Z. Chen, L. Hu, et al., Identification of safety gaps for fusion demonstration reactors, Nat. Energy 1 (2016) 16154.
[3] Y. Wu, Conceptual design of the China fusion power plant FDS-II, Fusion Eng. Des. 83 (2008) 1683–1689.
[4] Y. Wu, Development of high intensity D-T fusion neutron generator HINEG, Int. J. Energy Res. 42 (2018) 68–72.
[5] Q. Huang, N. Baluc, Y. Dai, et al., Recent progress of R&D activities on reduced activation ferritic/martensitic steels, J. Nucl. Mater. 442 (2013) 2–8.
[6] G. Aiello, J. Aktaa, F. Cismondi, et al., Assessment of design limits and criteria requirements for Eurofer structures in TBM components, J. Nucl. Mater. 414 (2011) 53–68.
[7] Q. Huang, C. Li, Q. Wu, et al., Progress in development of CLAM steel and fabrication of small TBM in China, J. Nucl. Mater. 417 (2011) 85–88.
[8] Q. Huang, Status and improvement of CLAM for nuclear application, Nucl. Fusion 57 (2017) (086042)(9pp).
[9] Q. Huang, F. Team, Development status of CLAM steel for fusion application, J. Nucl. Mater. 455 (2014) 649–654.
[10] Q. Wu, S. Zheng, S. Liu, et al., Effect of post-weld heat treatment on the mechanical properties of electron beam welded joints for CLAM steel, J. Nucl. Mater. 442 (2013) 512–517.
[11] C. Li, Q. Huang, P. Zhang, Effect of surface preparation on CLAM/CLAM hot isostatic pressing diffusion bonding joints, J. Nucl. Mater. 386–388 (2009) 550–552.
[12] Y. Wu, Design status and development strategy of China liquid lithium-lead blankets and related material technology, J. Nucl. Mater. 367 (2007) 1410–1415.
[13] A. Hishinuma, A. Kohyama, R. Klueh, et al., Current status and future R&D for reduced-activation ferritic/martensitic steels, J. Nucl. Mater. 258 (1998) 193–204.
[14] Q. Huang, S. Gao, Z. Zhu, et al., Progress in compatibility experiments on lithium-lead with candidate structural materials for fusion in China, Fusion Eng. Des. 84 (2009) 242–246.
[15] G. Yu, N. Nita, N. Baluc, Thermal creep behaviour of the EUROFER 97 RAFM steel and two European ODS EUROFER 97 steels, Fusion Eng. Des. 75 (2005) 1037–1041.
[16] B. Zhong, B. Huang, C. Li, et al., Creep deformation and rupture behavior of CLAM steel at 823 K and 873 K, J. Nucl. Mater. 455 (2014) 640–644.
[17] K. Shiba, H. Tanigawa, T. Hirose, et al., Development of the toughness-improved reduced-activation F82H steel for DEMO reactor, Fusion Sci. Technol. 62 (2012) 145–149.
[18] Z.X. Xia, C. Zhang, N.Q. Fan, et al., Improve creep properties of reduced activation steels by controlling precipitation behaviors, Mater. Sci. Eng. A 545 (2012) 91–96.
[19] L. Huang, X. Hu, W. Yan, et al., Laves-phase in the China low activation martensitic steel after long-term creep exposure, Mater. Des. 63 (2014) 333–335.
[20] H. Yao, F. Xuan, Z. Wang, et al., A review of creep analysis and design under multi-axial stress states, Nucl. Eng. Des. 273 (2007) 1969–1986.
[21] Y. Zhang, W. Jiang, S. Tu, et al., Creep crack growth behavior analysis of the 9Cr-1Mo steel by a modified creep-damage model, Mater. Sci. Eng. A 528 (2011) 6589–6595.
[22] L. Zhao, H. Jing, L. Xu, et al., Analysis of creep crack growth behavior of P92 steel welded joint by experiment and numerical simulation, Mater. Sci. Eng. A 558 (2012) 119–128.
[23] S. Tu, P. Segle, J. Gong, Creep demage and fracture of weldments at high temperature, Int. J. Press. Ves. Pip. 81 (2004) 199–209.
[24] ASTM E1457 Standard test method for measurement of creep crack growth times in metals, 2015.
[25] J. Pešička, R. Kužel, A. Dronhofer, et al., The evolution of dislocation density during heat treatment and creep of tempered martensite ferritic steels, Acta Mater. 51 (2003) 4847–4862.
[26] A. Aghajani, C. Somsen, G. Eggeler, On the effect of long-term creep on the microstructure of a 12% chromium tempered martensite ferritic steel, Acta Mater. 57 (2009) 5093–5106.

[27] A. Fedoseeva, N. Dudova, R. Kaibyshev, Creep behavior and microstructure of a 9Cr-3Co-3W martensitic steel, J. Nucl. Mater. 52 (2017) 2974–2988.
[28] H. Riedel, J. Rice, Tensile cracks in creeping solids, Fracture Mechanics, ASTM International, 1980.
[29] K.M. Nikbin, D.J. Smith, G.A. Webster, Prediction of creep crack-growth from uniaxial creep data, Proc. Soc. Lond. A Math. 396 (1984) 183–197.
[30] K. Nikbin, D. Smith, G. Webster, Prediction of creep crack growth from uniaxial creep data, Proc. R. Soc. Lond. A: Math. Phys. Eng. Sci. (1984) 183–197.
[31] A. Cocks, M. Ashby, Intergranular fracture during power-law creep under multiaxial stresses, Metal. Sci. 14 (1980) 395–402.
[32] K. Nikbin, D. Smith, G. Webster, An engineering approach to the prediction of creep crack growth, J. Eng. Mater. Technol. 108 (1986) 186–191.
[33] F.H. Norton, The Creep of Steel at High Temperatures, McGraw-Hill Book Company, Incorporated, 1929.
[34] F. Abe, Effect of fine precipitation and subsequent coarsening of Fe_2W Laves phase on the creep deformation behavior of tempered martensitic 9Cr-W steels, Metal. Mater. Trans. A 36 (2005) 321–332.
[35] F. Abe, Coarsening behavior of lath and its effect on creep rates in tempered martensitic 9Cr–W steels, Mater. Sci. Eng. A 387–389 (2004) 565–569.
[36] S. Liu, Q. Huang, L. Peng, et al., Microstructure and its influence on mechanical properties of CLAM steel, Fusion Eng. Des. 87 (2012) 1628–1632.
[37] K. Shiba, H. Tanigawa, T. Hirose, et al., Long-term properties of reduced activation ferritic/martensitic steels for fusion reactor blanket system, Fusion Eng. Des. 86 (2011) 2895–2899.
[38] P. Fernández, A.M. Lancha, J. Lapeña, et al., Creep strength of reduced activation ferritic/martensitic steel Eurofer'97, Fusion Eng. Des. 75–79 (2005) 1003–1008.
[39] A. Fedoseeva, E. Tkachev, V. Dudko, et al., Effect of alloying on interfacial energy of precipitation/matrix in high-chromium martensitic steels, J. Mater. Sci. 52 (2016) 4197–4209.
[40] M. Taneike, F. Abe, K. Sawada, Creep-strengthening of steel at high temperatures using nano-sized carbonitride dispersions, Nature 424 (2003) 294.